frontiers in Nanotechnology

ORIGINAL RESEARCH
published: 09 August 2021
doi: 10.3389/fnano.2021.710612

Insights on the Formation of Nanoparticles Prepared by Magnetron Sputtering Onto Liquids: Gold Sputtered Onto Castor Oil as a Case Study

Anastasiya Sergievskaya[1], Amy O'Reilly[1], Halima Alem[2], Julien De Winter[3], David Cornil[4], Jérôme Cornil[4] and Stephanos Konstantinidis[1]**

[1]Plasma-Surface Interaction Chemistry (ChIPS), University of Mons, Mons, Belgium, [2]Université de Lorraine, CNRS, Nancy, France, [3]Organic Synthesis and Mass Spectrometry Laboratory (S[2]MOs), University of Mons, Mons, Belgium, [4]Laboratory for Chemistry of Novel Materials (CMN), University of Mons, Mons, Belgium

OPEN ACCESS

Edited by:
Zheng Han,
Shanxi University, China

Reviewed by:
Xiao Xi Li,
Institute of Metals Research, Chinese Academy of Sciences (CAS), China
Simone Dal Zilio,
Consiglio Nazionale delle Ricerche (CNR), Italy

***Correspondence:**
Anastasiya Sergievskaya
anastasiya.sergievskaya@umons.ac.be
Stephanos Konstantinidis
stephanos.konstantinidis@umons.ac.be

Specialty section:
This article was submitted to Nanofabrication, a section of the journal Frontiers in Nanotechnology

Received: 16 May 2021
Accepted: 07 July 2021
Published: 09 August 2021

Citation:
Sergievskaya A, O'Reilly A, Alem H, De Winter J, Cornil D, Cornil J and Konstantinidis S (2021) Insights on the Formation of Nanoparticles Prepared by Magnetron Sputtering Onto Liquids: Gold Sputtered Onto Castor Oil as a Case Study. Front. Nanotechnol. 3:710612. doi: 10.3389/fnano.2021.710612

Magnetron sputter deposition of metal targets over liquids allows producing colloidal solutions of small metal nanoparticles (NPs) without any additional reducing or stabilizing reagents. Despite that this synthetic approach is known for almost 15 years, the detailed mechanism of NP formation is still unclear. Detailed investigations must be carried out to better understand the growth mechanism and, ultimately, control the properties of the NPs. Here, the combination of the gold (Au) target and castor oil, a highly available green solvent, was chosen as a model system to investigate how different experimental parameters affect the growth of NPs. The effect of deposition time, applied sputter power, working gas pressure, and type of sputter plasma (direct current magnetron sputtering (DC-MS) vs. high-power impulse magnetron sputtering (HiPIMS)) on properties of Au NPs has been studied by UV-vis spectroscopy and transmission electron microscopy (TEM), and further supported by quantum-chemistry calculations and mass-spectrometry analysis. The mechanism of the Au NP formation includes the production of primary NPs and their subsequent aggregative growth limited by diffusion in the viscous castor oil medium. Final Au NPs have a narrow size distribution and a medium diameter of 2.4–3.2 nm when produced in DC-MS mode. The NP size can be increased up to 5.2 ± 0.8 nm by depositing in HiPIMS mode which, therefore, mimics energy and time-consuming post synthesis annealing.

Keywords: Sputtering onto liquid, castor oil, gold nanoparticles, aggregative growth, HiPIMS

INTRODUCTION

The synthesis of nanomaterials has been intensely studied during the last few decades (Liz-Marzán, 2020). Thousands of experimental protocols have been reported for the production of colloidal dispersions of nanoparticles (NPs) and supercrystals having different sizes, shapes, and compositions (Boles et al., 2016; García-Lojo et al., 2019). These dispersions can be used for fabricating new materials with properties that are not available in traditional bulk component systems (Talapin et al., 2010; Kovalenko et al., 2015; Kagan et al., 2016). Typical recipe for the synthesis of metal NPs

includes reduction of the precursor (usually the metal salt) in certain solvent in the presence of capping molecules. The resulting colloidal solution contains metal NPs and other reaction products as well as the excess of the reducing reagents, so that the post-synthetic purification of NPs might be required for certain applications (Sebastian et al., 2014). In this respect, physical vapor deposition (PVD) onto liquid substrates is an alternative green approach allowing obtaining pure colloidal dispersions of metallic NPs containing only two components: the NP-forming atoms and the low-vapor pressure liquid that acts as a dispersion medium preventing fast agglomeration of NPs because of the high viscosity or/and the presence of stabilizing functional groups (Wender et al., 2013; Torimoto et al., 2016; Nguyen and Yonezawa, 2018). Although magnetron sputtering onto liquids is studied since 1996 with the work of Wagener et al. who produced silver NPs in silicone oil (Wagener et al., 1996), the mechanism of NP formation is not yet fully understood, although more than 100 papers dedicated to depositions on different liquids have been published. There are still open questions such as where does the nucleation process take place—on the liquid surface or in the bulk solution, what is the particle growth mechanism, why are the secondary growth processes more typical for certain NPs and host liquids, and how does the liquid affect the properties of the final NPs? These questions need to be answered to control better the NPs production and scale up the synthetic procedure for real-life applications. The way to go is to collect more quantitative information about NP synthesized via magnetron sputtering onto liquids under a wide range of controlled experimental conditions and analyze which factor(s) affect(s) the particle properties. The difficulty of today is also to compare the results obtained by different research groups due to the variety of sputter devices used and due to the absence of the full set of experimental conditions in the published papers (like deposition rates) which are mandatory information to reproduce completely NPs synthesis in different vacuum chambers or small sputter devices.

In this work we present new data on the formation of small, stable Au NPs in a castor oil. This vegetable oil is an unexpensive, highly available, nontoxic, green solvent that mainly consists of triglyceride of ricinoleic acid (~87%, see composition in **Supplementary Figure 1**) (Patel et al., 2016). Here, we discuss the systematic study of Au NP formation within a broad range of sputtering conditions. The effect of sputter time, applied power, argon pressure (from 0.07 to 2 Pa), and the type of sputtering plasma (Direct Current-Magnetron Sputtering (DC-MS) vs. High Power Impulse Magnetron Sputtering (HiPIMS)) on the behavior of colloidal solutions of Au NPs in castor oil has been studied by UV-vis spectroscopy during several months. The size and shape of the obtained NPs were characterized by TEM and the stability of colloidal solutions of Au NPs in castor oil was discussed in light of quantum-chemistry calculations and mass-spectrometry analysis. We believe that this massive new set of experimental data will open the way for the development of universal reproducible protocols of metal NP dispersions by magnetron sputter depositions onto liquids.

MATERIALS AND METHODS

Materials

Castor oil (CAS number 8001-79-4) was purchased from Alfa Aesar and used as received. Gold target (99.99%; 5.08 cm (2") in diameter; 1.59 mm (0.0625") in thickness; elastomer bonded to copper backing plate) was purchased from Kurt J. Lesker Company Ltd. and used as received.

Preparation of Colloidal Solutions of Au NPs

The sputtering procedure was similar to the previously reported in detail by our group (Sergievskaya et al., 2021). The schematic image of the vacuum chamber can be found in **Supplementary Figure 2**. The main deposition chamber, i.e., where sputtering takes place, was permanently pumped down to the pressure of 10^{-6} Pa. In a typical experiment, 4.0 g of castor oil placed into a cylindrical plastic beaker (3 cm in height; 2.8 cm in diameter) were degassed inside the load-lock chamber until the pressure of 10^{-5} Pa was reached. After this, the sample was transferred into the deposition chamber. The argon pressure was precisely controlled by a throttle valve placed in front of the turbomolecular pump. The working distance between the target and liquid surfaces was equal to 20 cm. Depositions lasted 10 min for all cases except when studying the effect of the sputter time. The magnetron was cooled by water line, hence allowing stable deposition conditions. Depositions in DC-MS regime were done with commercial power supply (Advanced Energy MDX 500), while for HiPIMS experiments a prototype constructed in MATERIA NOVA R&D center (Britun et al., 2018)) was used. In this case magnetron sputtering was carried out at an argon pressure of 0.7 Pa, at a time-averaged sputter power of 80 W (current 92 mA; voltage 867 V), and with the following pulse parameters (pulse repetition frequency 800 Hz, pulse duration 20 μs; peak target current density 0.3 A/cm^2). Typical current and voltage waveforms can be found in Britun et al. (2018).

All the samples were photographed after venting the load-lock chamber and immediately stirred at the magnetic stirrer for 5 min. A detailed set of experimental conditions for each deposition can be found in **Supplementary Table 1** in the Supplementary material. The concentration of deposited gold atoms in colloidal solutions was estimated based on gold flux measurement (experimental procedure and obtained values can be found in the Supplementary material in **Supplementary Table 2** and in **Supplementary Figure 3**).

Characterization Methods

Colloidal dispersion of Au NPs obtained via magnetron sputtering of gold target onto castor oil was regularly characterized by means of UV-vis spectroscopy with Agilent Cary 5000 UV-vis-NIR spectrometer. The shape, size, and size distributions of particles were determined by transmission electron microscopy (TEM) with Philips CM200 microscope. The castor oil composition before and after exposure to the argon-based plasma was analyzed by Positive-ion Matrix assisted LASER Desorption/Ionization-Mass Spectrometry (MALDI-MS) with Waters QToF Premier mass spectrometer.

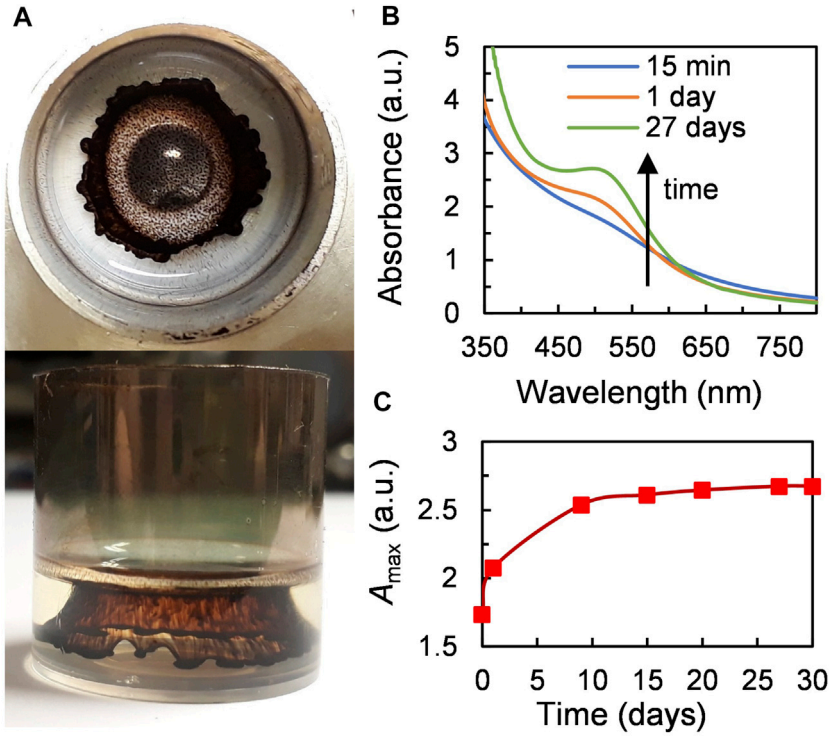

FIGURE 1 | A typical sample produced by magnetron sputtering of gold onto castor oil. **(A)** Photographs of the sample just after venting the vacuum chamber (experimental conditions: Ar pressure–0.07 Pa, applied power–80 W (488 V, 162 mA), sputter time–5 min). **(B)** UV-vis spectra of the solution obtained after stirring the sample (time marks indicate the time after finishing sputtering). **(C)** Increase in absorbance at the maximum of SPR of Au NPs (505 nm) with time.

Additional information about characterization methods can be found in the Supplementary material.

Density Functional Theory Calculations

To better understand the chemical interactions between the castor oil components and Au NPs, quantum-chemical calculations were carried out at the density functional theory (DFT) and density functional tight-binding (DFTB) levels in two steps, as done in our previous paper (Sergievskaya et al., 2021). A detailed protocol leading to the interaction energy values is placed in the Supplementary material.

RESULTS AND DISCUSSION

Reproducibility of the Synthesis and Stability of the Products

Formation of Au NPs after magnetron sputtering of gold target onto castor oil was first observed with the naked eye. As can be seen in **Figure 1A**, a jellyfish-like brownish cloud of particles was formed under the oil surface. The size and color intensity of this cloud is proportional to the amount of gold deposited during the experiment. Transparent colloidal dispersions were obtained after stirring the samples. The color of the solutions changed from brown to red with storage time. As depicted in the UV-vis spectra in **Figure 1B** no surface plasmon resonance (SPR) band was observed 15 min after sputter deposition. However, the formation of well-developed SPR band with maximum at 505 nm started 1 day after stirring the sample. The absorbance reached its maximum located at 505 nm 3 weeks after the synthesis (see **Figure 1C**). An increase in absorbance might be explained by secondary growth processes taking place in the solution after sputter deposition is over. Such a behavior of Au NPs has been mentioned by other research groups performing magnetron sputtering onto ionic liquids (Vanecht et al., 2011, 2012; Hamm et al., 2014), PEEL (Shishino et al., 2011), PEGs (Slepička et al., 2015), and oleic acid (Nguyen et al., 2020).

To check the reproducibility of sputter experiments, several depositions were made on different days but under similar experimental conditions. At first, the samples look similar with the naked (see **Supplementary Figure 5A**) but to analyze the reproducibility in a more rigorous way the UV-vis spectra of two samples 3.1 and 3.2 were recorded 15 min after venting the vacuum chamber and stirring and compared. The two absorbance curves are superimposed (**Supplementary Figure 5B**). On the same graph, we also verified the UV-vis spectra of the solutions recorded 24 h after stirring. The curves have the same shape but sample 3.1 has an absorbance at 505 nm 3.8% higher than the one of sample 3.2. However, this is not a significative variation for colloidal systems with secondary growth processes. Nevertheless, even though there is a marginal variation in the UV-vis spectra after sputtering, all the experiments were performed under time-controlled conditions. TEM characterization was done after all the samples reached the maximum absorbance.

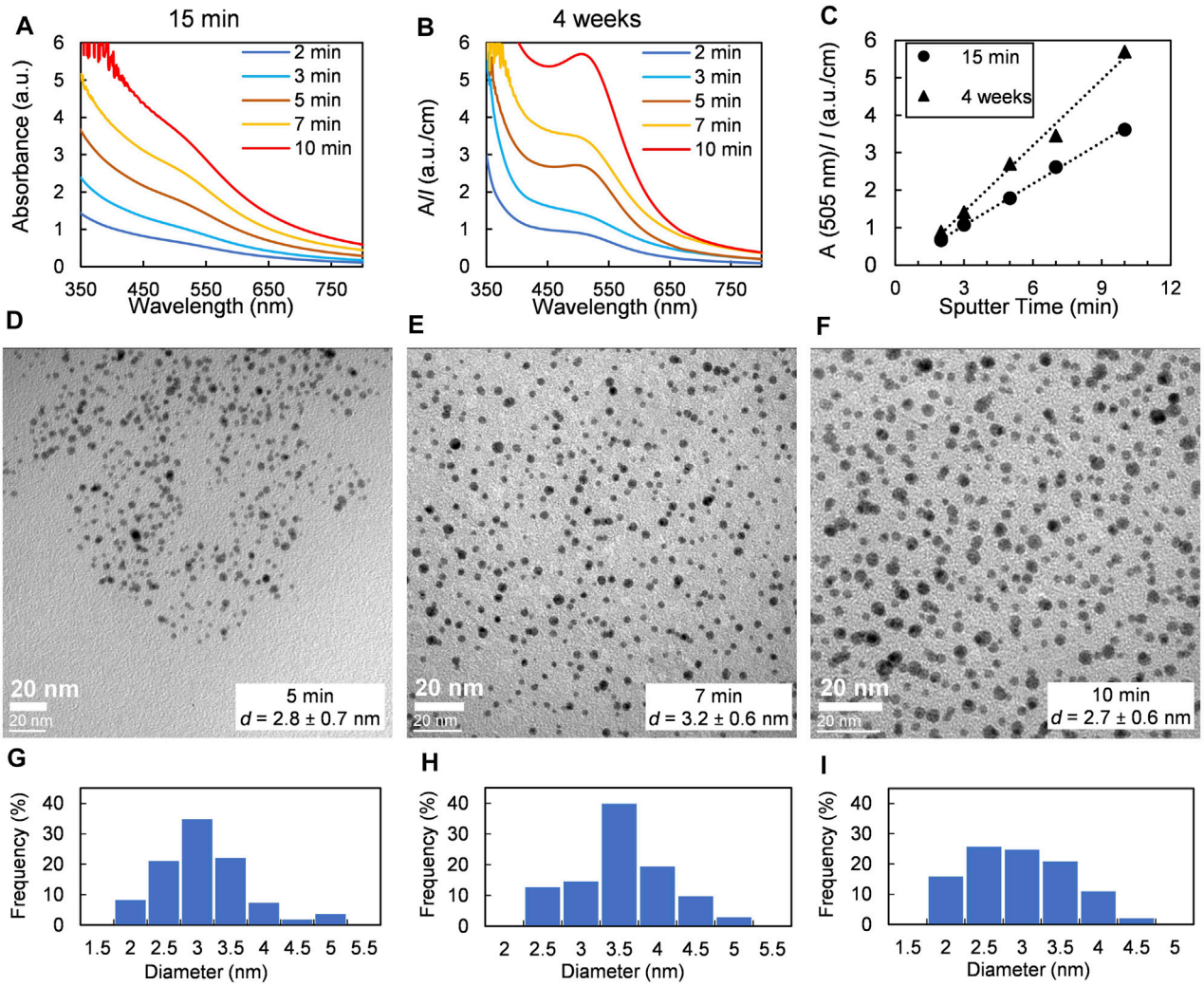

FIGURE 2 | Effect of sputter time: samples were obtained at a fixed argon pressure of 0.07 Pa and an applied power of 80 W. **(A)** and **(B)** UV-vis spectra of dispersions of Au NPs in castor oil recorded 15 min and 4 weeks later after deposition, respectively. **(C)** Changes in absorbance at the maximum of SPR band of Au NPs. **(D–F)** TEM images and **(G–I)** size distributions of Au NPs obtained at sputter time of 5, 7, and 10 min, respectively.

Dispersions of Au NPs obtained via magnetron sputtering onto castor oil have a good colloidal stability. 25 depositions were made and no decrease in the absorbance at maximum SPR band or precipitation was noticed during at least one year for 23 of them, the energetic position of SPR stayed also constant during this period. Heating of the samples to 100 C for 2 h does not cause any significant changes in UV-vis spectra (**Supplementary Figure 6**) and does not provoke aggregation.

MALDI-mass spectrometry analyses of castor oil before and after plasma treatment have been done. As presented in **Supplementary Figure 7**, beside a slight oxidation, there is no significant modification of the chemical composition of the substrate (the host liquid) during the deposition with the DC-MS procedure. According to the results of quantum-chemical calculations performed at the DFT and DFTB levels, the chemical interactions between the triglyceride of ricinoleic acid, i.e., the main castor oil component, and the surfaces of Au NPs are favorable. As a matter of fact, the interaction energy between the model molecule, 1/3 part of triglyceride of ricinoleic acid, and the Au 111) surface is negative (−0.14 eV) (see **Supplementary Figure 4**). In our previous work, the interaction energy between the same model module molecule and the Ag 111) surface was positive, and colloidal solutions of Ag NPs in castor oil produced by magnetron sputtering were indeed not stable (Sergievskaya et al., 2021). These new data imply that castor oil is a good capping agent for Au NPs.

All the data reported above prove that magnetron sputter deposition of a gold target onto castor oil allows producing stable colloidal solutions of Au NPs.

Effect of Sputter Time

Under fixed sputter conditions the gold flux is constant so that an increase in sputter time leads to an increase in the number of gold atoms deposited onto the liquid surface. The size and

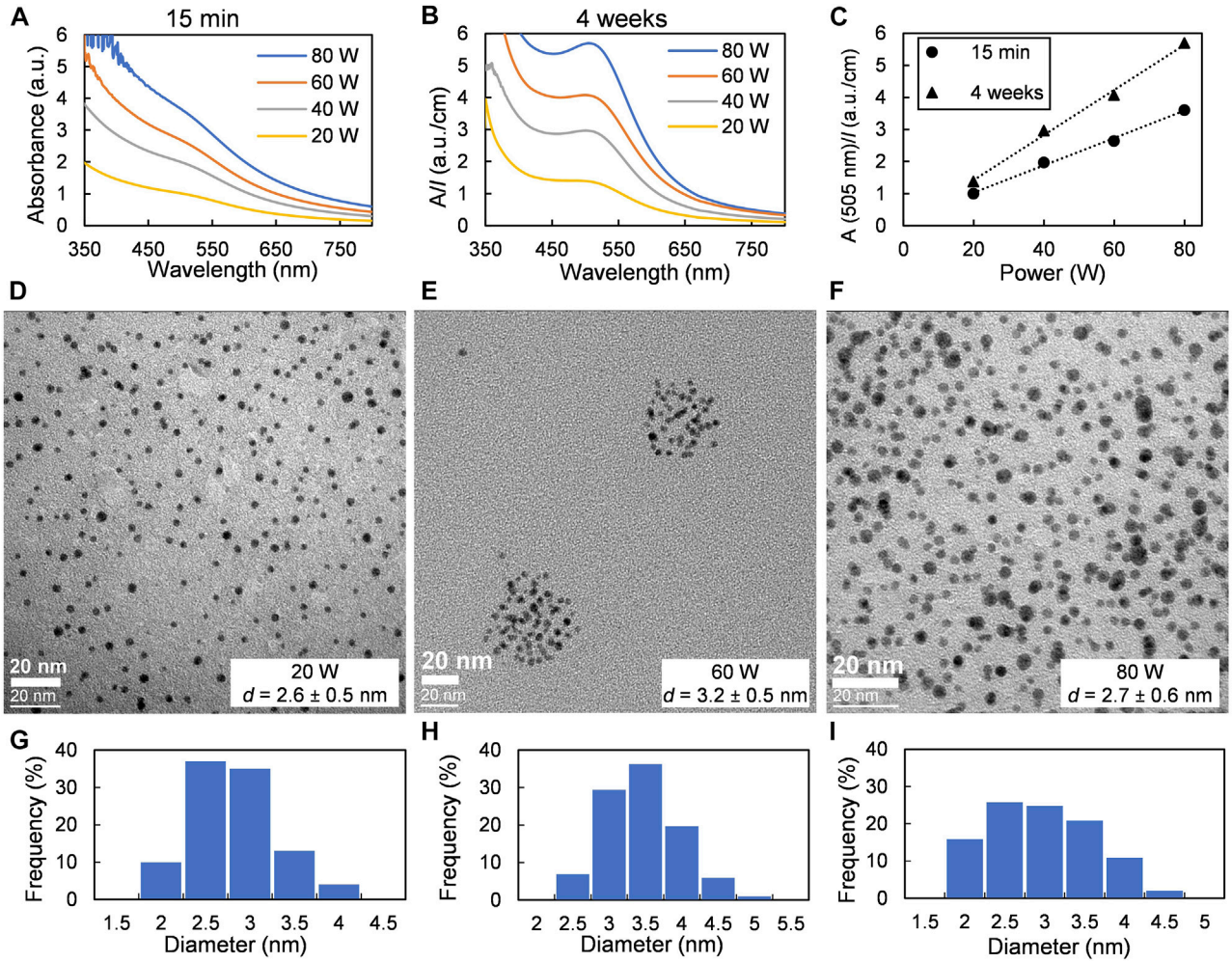

FIGURE 3 | Effect of applied power: samples were obtained at a fixed argon pressure of 0.07 Pa and a sputter time of 10 min. **(A)** and **(B)** UV-vis spectra of dispersions of Au NPs in castor oil recorded 15 min and 4 weeks after deposition, respectively. **(C)** Changes in absorbance at the maximum of SPR band of Au NPs. **(D–F)** TEM images and **(G–I)** size distributions of Au NPs obtained at sputter power of 20, 60, and 80 W, respectively.

the color intensity of the Au NPs cloud under the castor oil surface significantly increases with sputter time (**Supplementary Figure 8**). As seen in **Figures 2A,B**, the absorbance of colloidal solutions obtained after stirring of the samples increases linearly with sputter time. The fact that this dependence stays linear 4 weeks after sample preparation means that the aging of Au NPs goes synchronically. Different research groups have already shown that sputter time does not affect the size of metal NPs but increases their concentration inside the host liquid solution (Torimoto et al., 2006; Suzuki et al., 2009; Shishino et al., 2010; Tsuda et al., 2010; Hatakeyama et al., 2011; Slepička et al., 2015; Sumi et al., 2015; Lee et al., 2018; Sergievskaya et al., 2021). According to TEM images (see **Figures 2D–F**), obtained Au NPs have spherical shape and narrow size distribution (**Figures 2G–I**); the mean diameter of Au NPs in castor oil is independent of sputter time or gold concentration.

Effect of Sputter Power

An increase in sputter power leads to an increase in gold deposition flux (see **Supplementary Figure 3A**). The size of the NP cloud under the oil surface increased with sputter power as well as the color intensity of obtained colloidal dispersions (**Supplementary Figure 9**). One can see a linear increase in absorbance of the colloidal solutions when changing the sputter power from 20 to 80 W, i.e., for power densities equal to 1 and 4W/cm^2 (**Figures 3A,B**). The dependence of absorbance at 505 nm (the maximum of SPR band of Au NPs) vs power stays linear both 15 min and 1 month after sample preparation (**Figure 3C**). The size of the obtained NPs does not depend on sputter power and is approximately 2.6–3.2 nm (see **Figures 3D–I**). The fact that discharge current or power, or more straightforwardly, the deposition flux, does not affect the size of metal NPs obtained via sputtering onto liquids has been noticed before by us (Sergievskaya et al., 2021) and other research groups (Hatakeyama et al., 2011; Sumi et al., 2015; Qadir et al., 2019).

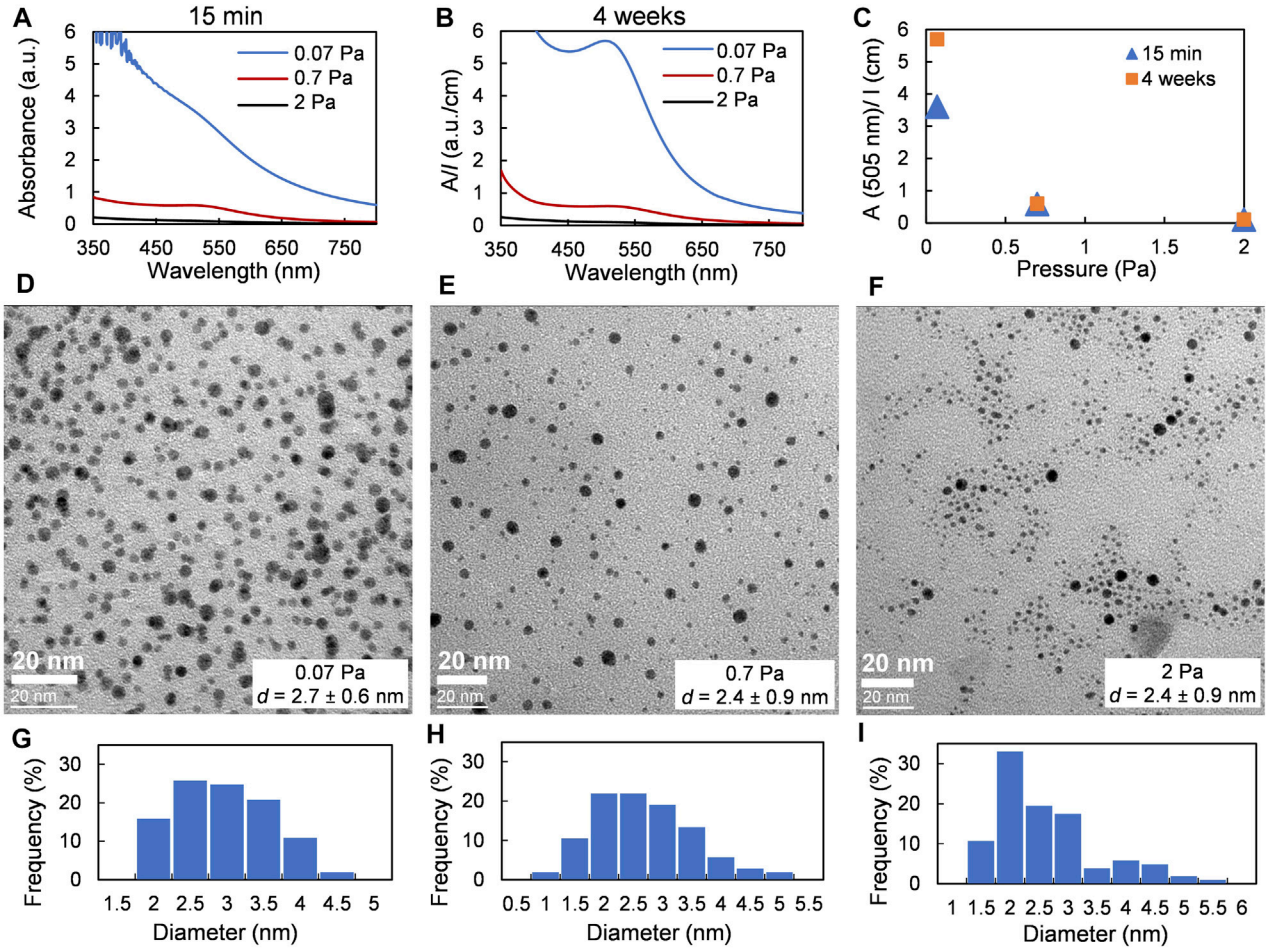

FIGURE 4 | | Effect of argon pressure. Samples were obtained at a fixed applied power of 80 W and a sputter time of 10 min. **(A)** and **(B)** UV-vis spectra of dispersions of Au NPs in castor oil recorded 15 min and 4 weeks after deposition, respectively **(C)** Changes in absorbance at the maximum of SPR band of Au NPs. **(D–F)** TEM images and **(G–I)** size distributions of Au NPs obtained at argon pressure of 0.07, 0.7, and 2 Pa, respectively.

Therefore, it can be reasonably assumed that the variation of the sputter power does not provoke any significant alteration of the nucleation and growth conditions of the gold NPs, in our experimental conditions. However, some scientists reported an increase in the NP size with discharge voltage (Suzuki et al., 2009; Wender et al., 2010, 2011; Sugioka et al., 2015). This behavior might be explained by the heating of the host liquid by plasma-born species and sputtered metal atoms and the IR radiations emitted by the target during the deposition (Orozco-Montes et al., 2021). For example, it has been recently shown that the temperature of 4 ml of glycerol was increased by 17°C during 20 min platinum deposition with 12 cm of working distance (100 W; 5 W/cm^2) and by 40°C with 5 cm of working distance at the same DC power density (Orozco-Montes et al., 2021). An increase in liquid temperature leads to a decrease in both the viscosity and surface tension of the host liquid, so that the sputter atoms more easily penetrate under the liquid surface and the number of collisions between freshly solvated sputtered atoms and primary clusters formed under the liquid surface increases. As a result, NPs of larger size might form.

Effect of Argon Pressure

An increase in pressure leads to a significant decrease in gold flux (see **Supplementary Figure 3B**) but also in the kinetic energy of the sputtered atoms reaching the liquid surface because of increased gas phase scattering. It was seen with the naked eye that the area of deposited material drastically decreased with pressure at a fixed sputter time of 10 min (**Supplementary Figure 10A**). Consequently, the color of the colloidal solution obtained after stirring the sample produced at 2 Pa was almost yellow. No strong SPR resonance band was observed in UV-vis spectra of initial or aged solutions in this condition (2 Pa–**Figure 4A**); however, the SPR peak appeared with time for samples prepared at a pressure of 0.07 and 0.7 Pa (**Figure 4B**). The UV-vis spectrum of 2 Pa sample did not change significantly even one month after the preparation of the solution; the increase in absorbance at 505 nm was about 5% (**Figure 4C**). The size of NPs was measured by TEM 10 months after the sputtering procedure; it was found that the mean diameter of the final Au NPs does not depend on gas pressure (see **Figures 4D–I**). The effect of argon pressure on metal NP size obtained by sputtering

onto liquids has been already studied in three works (Wagener et al., 1996; Orozco-Montes et al., 2021; Sergievskaya et al., 2021), showing in all the cases that the size of NPs increased with argon pressure. The fact that NPs produced in this work was in a range of 2.4–2.7 nm might be explained by the difference in concentrations of the deposited gold atoms. A large number of small gold clusters form initially at a pressure of 0.07 Pa and their size increased because of the collisions during the storage time, as can be seen by UV-vis spectroscopy (**Figures 4A–C**). In contrast, at 0.7 and 2 Pa pressure, since the total concentration of deposited gold is lower at a higher pressure, a smaller number of larger particles form. These particles will collide less frequently in a viscous oil medium.

The sample obtained at a pressure of 2 Pa allows us to compare Au NPs obtained in the frame of this work with the results provided in Wender et al. (2010) (see the list of experimental parameters in **Supplementary Table 3**). In both the cases, Au NPs have a spherical shape with a mean diameter of 2.4 ± 0.9 nm (this work) vs. 3.8 ± 1.1 nm (Wender et al., 2010). The larger size of Au NPs produced by Wender might be explained by the fact that the deposition rate was higher so that more primary gold clusters were formed in smaller volume of castor oil and led to the formation of larger NPs. The difference in the deposition conditions might also lead to different liquid heating rates. Indeed, the modeling of the metal flux reaching the liquid surface with the SIMTRA Monte Carlo-based simulation package (Van Aeken et al., 2008; Depla and Leroy, 2012) has shown that obtained energy flux is dramatically increased in case of work (Wender et al., 2010). Considering that the thickness of the oil layer was 3 times less in case of Wender's research, it might be assumed that in that case the liquid substrate was heated much more efficiently than in case of the present work after the same treatment duration of 10 min. Decreasing in viscosity with the increase in oil temperature made diffusion faster, hence promoting collisions inside the liquid and allowing the formation of larger Au NPs. According to Wender et al. (2011), solutions of Au NPs in castor oil were stable about 8 months while our samples demonstrated a similar UV-vis spectrum for 14 months after the solutions reached the maximum of absorption.

Effect of Plasma Type: DC-MS vs. HiPIMS

Changing the power supply from DC-MS to HiPIMS allows us to deposit metal ions instead of metal neutrals. During DC-MS deposition, the film-forming species, i.e., metal neutrals, have kinetic energy typically in the range of several eV (Depla, 2013), but in the case of HiPIMS discharges, metal ions have kinetic energy of several tens of eV (Sarakinos et al., 2010). Such species might cause the heating up of the top liquid layer and penetrate deeper in the bulk solution, and hence affect the properties of NPs (Sergievskaya et al., 2021). HiPIMS power supplies were used only twice for sputtering onto liquids: during the deposition of Cr-Mn-Fe-Co-Ni alloy onto BMIM-TFSI ionic liquid (Garzón-Manjón et al., 2018) and by us for depositing silver onto castor oil (Sergievskaya et al., 2021). In both cases, the size of particles obtained with HiPIMS plasmas was larger than with DC-MS ones.

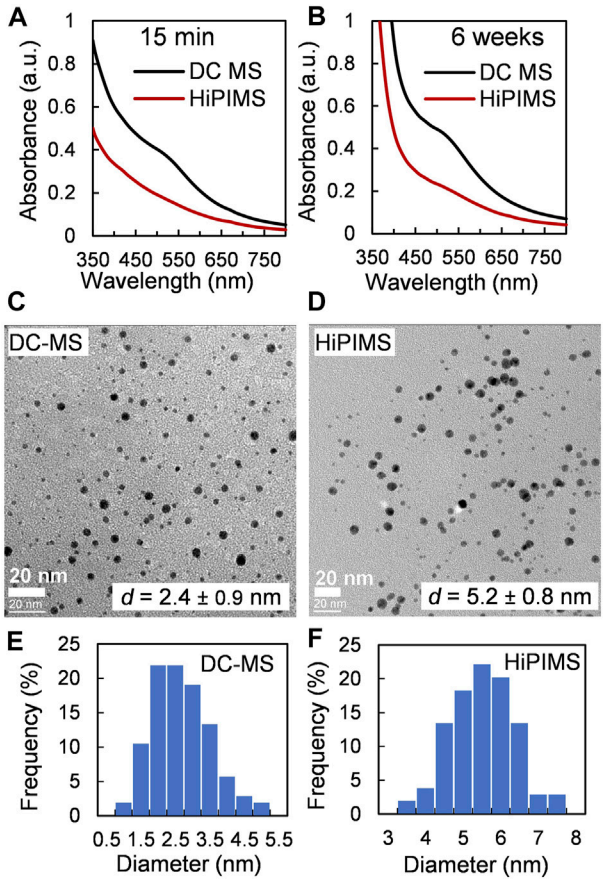

FIGURE 5 | Effect of plasma type: samples were obtained at a fixed argon pressure of 0.7 Pa and a sputter time of 10 min. **(A)** and **(B)** UV-vis spectra of dispersions of Au NPs in castor oil recorded 15 min and 6 weeks after deposition, respectively. **(C, D)** TEM images and **(E, F)** size distributions of Au NPs obtained with DC-MS and HiPIMS power supplies, respectively.

The photographs of the samples produced with DC-MS and HIPIMS power supplies can be found in **Supplementary Figure 11A**. One can see with the naked eye that the size of the NP cloud is smaller in case of the HiPIMS mode. This might be explained by the lower gold flux (see **Supplementary Table 2**). All colloidal solutions obtained after stirring of the HiPIMS samples were transparent and had brownish color (**Supplementary Figure 11B**). No strong SPR band appeared in the UV-vis spectra of HiPIMS samples even after one-month storage time (**Figures 5A,B**). Even though in case of the HiPIMS regime the concentration of gold in the solution was almost twice lower than in the DC-MS regime, the size of final gold NPs was larger: 5.2 ± 0.8 nm (HiPIMS) vs. 2.4 ± 0.9 nm (DC-MS), **Figures 5C–F**. This increase in NP size might be explained once again by the heating up of the host liquid by the HiPIMS plasma as discussed previously in Sergievskaya et al. (2021). Thus, the number of collisions between forming primary gold clusters increases and larger NPs are expected to form. Because the high-kinetic energy ions present in HiPIMS plasma might affect the host liquid components, the characterization of castor oil before and after exposure to the

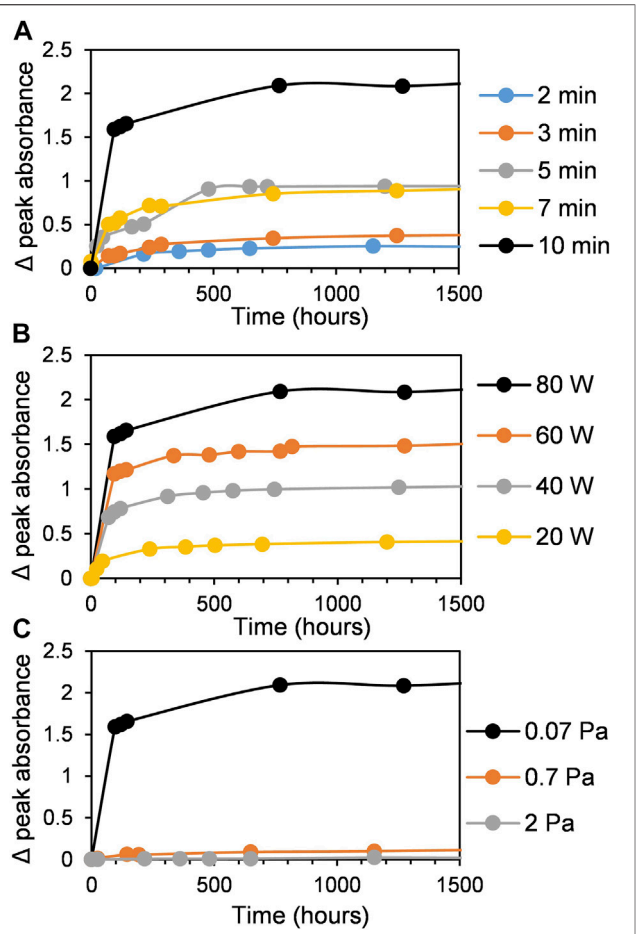

FIGURE 6 | The evolution of the absorbance at the maximum of SPR band (505 nm) as a function of time. **(A)** Effect of sputter time, **(B)** effect of sputter power, and **(C)** effect of argon pressure.

plasma was done by MALDI-mass spectrometry. Owing to a more aggressive treatment, some changes in oil structure were observed (**Supplementary Figure 7**). Even if an additional detailed future research is needed to explain the mechanism of oil degradation process, it is more probably due to successive oxidation reactions that could correspond to the 16 mass units difference observed in the mass spectrum. The here-provided data show once again that 1-step deposition with HiPIMS power supply might be used as an alternative to the 2-step process when primed metal NPs produced in the DC-MS regime were annealed with the aim of increasing their size (Meischein et al., 2019; Chauvin et al., 2020).

Mechanism of Nanoparticle Formation

The growth of metal NPs produced by reduction of metal ions in solution is much more studied than the formation of NPs during the magnetron sputtering process due to the absence of *in situ* observations inside the vacuum chamber. For the wet-chemistry synthesis, the kinetic curves representing the growth of metal NPs have a sigmoidal shape with an induction period corresponding to the nucleation step (Watzky and Finke, 1997; Finney and Finke, 2008). According to works reported in Ref. (Watzky and Finke, 1997, 2018; Finney and Finke, 2008; Sergievskaya et al., 2015), an autocatalytic growth step follows the nucleation process which leads to the formation of primary metal NPs. Secondary growth processes such as aggregation, coalescence, or Ostwald ripening might also take place in the solution (Finney et al., 2012; Thanh et al., 2014; Wang et al., 2014). In contrast to the classical colloidal synthesis, the concentration of metal in the solution is not constant in the case of sputtering onto liquid processes; it increases with sputtering time. Moreover, in case of sputtering onto still host liquid (without stirring), the obtained solutions are not homogeneous (see **Figure 1A**). Because of the rather high kinetic energy of the gold atoms (which depends on the working conditions), these species might reach the liquid subsurface and the nucleation and growth processes would then occur in the bulk solution. Small primary gold clusters with size less than 2 nm form during this time. There is no induction period on the typical kinetic curve shown in **Figure 1C** since the sample characterization was done after venting of the vacuum chamber. In view of the absence of a strong SPR band in the UV-vis spectra of colloidal solutions of AuNPs obtained after the sample stirring, we believe that the concentration of small gold clusters (<2 nm) stays high. We cannot exclude the presence of small amount of Au atoms stabilized by castor oil in the mixture. As the peak absorption of the SPR band increases with time (see **Figure 6**), one can see that, during the first week, the concentration of larger Au NPs is growing faster in case of more concentrated solutions. This process gets significantly slower with time. These findings lead to the hypothesis that the growth process is limited by the diffusion of the primary clusters in the castor oil (**Figure 7**). The clusters and atoms remaining after the nucleation processes aggregate and form larger Au NPs. Moreover, this aggregation process might have an autocatalytic nature (Finney et al., 2012; Wang et al., 2014). Finally, we stress that the growth of Au NPs after the end of the magnetron sputter deposition process has already been considered in previous works in the frame of aggregative models (Shishino et al., 2011; Vanecht et al., 2011, 2012; Hamm et al., 2014; Slepička et al., 2015).

To estimate the growth process rate, we plotted graphs in the coordinates ln (a/(1-a)) *vs.* t, where a is A_t/A_{max} (normalized absorbance) and t is the time after the end of the deposition process. The observed rate constants, k_{obs}, were determined from

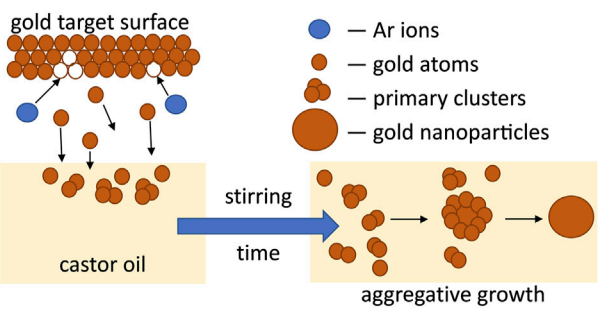

FIGURE 7 | Scheme of the formation of Au NPs after magnetron sputtering of gold target onto castor oil.

the slope of the curves (see **Supplementary Figure 12**) as it was done before in other works (Esumi et al., 2000; Harada and Inada, 2009; Mohamed et al., 2011). Such an approach describes only approximately 50% of the kinetic curves (Watzky and Finke, 2018) from **Figure 6**, i.e., the part of aggregative growth of Au NPs. As expected for an aggregation process in such a viscous medium such as castor oil (0.650 Pas (Patel et al., 2016)), k_{obs} are in the range of $(1–10)\cdot10^{-7}$ s^{-1} (see **Supplementary Table 1**) and slightly increase with gold concentration (**Supplementary Figure 13**). The values of k_{obs} estimated in less viscous aqueous solutions are usually much higher (approximately 10^{-3} s^{-1} or more (Esumi et al., 2000)) due to fast diffusion of reactive species and high concentrations of reducing reagents. However, in the case of sputtering onto the liquid procedure, there are no reducers; thus, the process rate is limited by the diffusion and coalescence between primary particles inside the vegetable oil. For a more precise analysis, a larger set of kinetic data, including the nucleation period, is needed.

CONCLUSION

1Magnetron sputtering of a gold target onto low-cost, nontoxic, vegetable castor oil allows us to obtain stable colloidal solutions of small spherical Au NPs. It was clearly shown that a brownish cloud forms underneath the oil surface during the deposition process onto still liquids. Stirring of the obtained systems leads to the formation of transparent colloidal solutions containing the primary gold clusters with diameter less than 2 nm according to their UV-vis spectra. The Au NPs grow with time due to aggregation of primary clusters and sputtered atoms; the process is limited by diffusion in the viscous oil medium. The size of the final Au NPs does not depend on sputter time, sputter power, or argon pressure, and the mean diameter stays in a range of 2.4–3.2 nm for the DC-MS mode, while deposition with HiPIMS power supply allows us to produce Au NPs with size of 5.2 ± 0.8 nm. The HiPIMS-related data set and the comparison with previously published work for which the plasma parameters were different provide insight on the influence of the heating of the host liquid during the plasma process, and the subsequent formation of larger NPs. Our results show that magnetron sputter deposition onto vegetable oils is an effective green technique to produce stable colloidal solutions of small NPs. These dispersions might be used in further (environmentally friendly plasma-based) polymerization processes for the production of composite polymers.

DATA AVAILABILITY STATEMENT

The original contributions presented in the study are included in the article/**Supplementary Material**, further inquiries can be directed to the corresponding authors.

AUTHOR CONTRIBUTIONS

AS and AO performed the synthesis of nanoparticles, its characterization by UV-vis spectroscopy and the analysis of experimental data. HA performed the characterization of the products by TEM. JW was responsible for MALDI analysis. AS, DC, and JC were responsible for the DFT calculations. SK was responsible for the work conceptualization, SIMTRA simulations and project supervision. AS wrote the original draft of the manuscript, all the authors were actively involved in the manuscript editing.

FUNDING

SK and JC are senior research associate and research director of the National Fund for Scientific Research (F.R.S.-FNRS, Belgium), respectively. SK and AS thank the FNRS for the financial support through the "SOLUTIoN" project No T.0134.19. The DFT calculations were supported by the Consortium des Équipements de Calcul Intensif (CÉCI), funded by the Fonds National de la Recherche Scientifique (F.R.S.-FNRS) under Grant No. 2.5020.11. The S^2MOs lab is grateful to the Fonds National de la Recherche Scientifique (F. R. S.-FNRS) for financial support for the acquisition of the Waters QTof Premier mass spectrometer.

ACKNOWLEDGMENTS

Authors would like to thank Dany Cornelissen for the excellent vacuum chamber maintenance.

SUPPLEMENTARY MATERIAL

The Supplementary Material for this article can be found online at: https://www.frontiersin.org/articles/10.3389/fnano.2021.710612/full#supplementary-material.

REFERENCES

Boles, M. A., Engel, M., and Talapin, D. V. (2016). Self-Assembly of Colloidal Nanocrystals: From Intricate Structures to Functional Materials. *Chem. Rev.* 116, 11220–11289. doi:10.1021/acs.chemrev.6b00196

Britun, N., Michiels, M., Godfroid, T., and Snyders, R. (2018). Ion Density Evolution in a High-Power Sputtering Discharge With Bipolar Pulsing. *Appl. Phys. Lett.* 112, 234103. doi:10.1063/1.5030697

Chauvin, A., Sergievskaya, A., El Mel, A.-A., Fucikova, A., Antunes Corrêa, C., Vesely, J., et al. (2020). Co-Sputtering of Gold and Copper onto Liquids: A Route towards the Production of Porous Gold Nanoparticles. *Nanotechnology* 31, 455303. doi:10.1088/1361-6528/abaa75

Depla, D., and Leroy, W. P. (2012). Magnetron Sputter Deposition as Visualized by Monte Carlo Modeling. *Thin Solid Films* 520, 6337–6354. doi:10.1016/j.tsf.2012.06.032

Depla, D. (2013). Magnetrons, Reactive Gases and Sputtering. Diederik Depla Available at: https://biblio.ugent.be/publication/4239033 (Accessed February 08, 2021).

Esumi, K., Hosoya, T., Suzuki, A., and Torigoe, K. (2000). Formation of Gold and Silver Nanoparticles in Aqueous Solution of Sugar-Persubstituted Poly(Amidoamine) Dendrimers. *J. Colloid Interf. Sci.* 226, 346–352. doi:10.1006/jcis.2000.6849

Finney, E. E., and Finke, R. G. (2008). Nanocluster Nucleation and Growth Kinetic and Mechanistic Studies: A Review Emphasizing Transition-Metal Nanoclusters. *J. Colloid Interf. Sci.* 317, 351–374. doi:10.1016/j.jcis.2007.05.092

Finney, E. E., Shields, S. P., Buhro, W. E., and Finke, R. G. (2012). Gold Nanocluster Agglomeration Kinetic Studies: Evidence for Parallel Bimolecular Plus Autocatalytic Agglomeration Pathways as a Mechanism-Based Alternative to an Avrami-Based Analysis. *Chem. Mater.* 24, 1718–1725. doi:10.1021/cm203186y

García-Lojo, D., Núñez-Sánchez, S., Gómez-Graña, S., Grzelczak, M., Pastoriza-Santos, I., Pérez-Juste, J., et al. (2019). Plasmonic Supercrystals. *Acc. Chem. Res.* 52, 1855–1864. doi:10.1021/acs.accounts.9b00213

Garzón-Manjón, A., Meyer, H., Grochla, D., Löffler, T., Schuhmann, W., Ludwig, A., et al. (2018). Controlling the Amorphous and Crystalline State of Multinary Alloy Nanoparticles in an Ionic Liquid. *Nanomaterials* 8, 903. doi:10.3390/nano8110903

Hamm, S. C., Basuray, S., Mukherjee, S., Sengupta, S., Mathai, J. C., Baker, G. A., et al. (2014). Ionic Conductivity Enhancement of Sputtered Gold Nanoparticle-In-Ionic Liquid Electrolytes. *J. Mater. Chem. A.* 2, 792–803. doi:10.1039/C3TA13431H

Harada, M., and Inada, Y. (2009). *In Situ* Time-Resolved XAFS Studies of Metal Particle Formation by Photoreduction in Polymer Solutions. *Langmuir* 25, 6049–6061. doi:10.1021/la900550t

Hatakeyama, Y., Onishi, K., and Nishikawa, K. (2011). Effects of Sputtering Conditions on Formation of Gold Nanoparticles in Sputter Deposition Technique. *RSC Adv.* 1, 1815–1821. doi:10.1039/c1ra00688f

Kagan, C. R., Lifshitz, E., Sargent, E. H., and Talapin, D. V. (2016). Building Devices from Colloidal Quantum Dots. *Science* 353, aac5523. doi:10.1126/science.aac5523

Kovalenko, M. V., Manna, L., Cabot, A., Hens, Z., Talapin, D. V., Kagan, C. R., et al. (2015). Prospects of Nanoscience with Nanocrystals. *ACS Nano* 9, 1012–1057. doi:10.1021/nn506223h

Lee, S. H., Jung, H. K., Kim, T. C., Kim, C. H., Shin, C. H., Yoon, T.-S., et al. (2018). Facile Method for the Synthesis of Gold Nanoparticles Using an Ion Coater. *Appl. Surf. Sci.* 434, 1001–1006. doi:10.1016/j.apsusc.2017.11.008

L. Liz-Marzán (Editors) (2020). *Colloidal Synthesis of Plasmonic Nanometals* (New York: Jenny Stanford Publishing). doi:10.1201/9780429295188

Meischein, M., Garzón-Manjón, A., Frohn, T., Meyer, H., Salomon, S., Scheu, C., et al. (2019). Combinatorial Synthesis of Binary Nanoparticles in Ionic Liquids by Cosputtering and Mixing of Elemental Nanoparticles. *ACS Comb. Sci.* 21, 743–752. doi:10.1021/acscombsci.9b00140

Mohamed, H. H., Dillert, R., and Bahnemann, D. W. (2011). Growth and Reactivity of Silver Nanoparticles on the Surface of TiO2: A Stopped-Flow Study. *J. Phys. Chem. C* 115, 12163–12172. doi:10.1021/jp2031576

Nguyen, M. T., and Yonezawa, T. (2018). Sputtering Onto a Liquid: Interesting Physical Preparation Method for Multi-Metallic Nanoparticles. *Sci. Technol. Adv. Mater.* 19, 883–898. doi:10.1080/14686996.2018.1542926

Nguyen, M. T., Wongrujipairoj, K., Tsukamoto, H., Kheawhom, S., Mei, S., Aupama, V., et al. (2020). Synergistic Effect of the Oleic Acid and Oleylamine Mixed-Liquid Matrix on Particle Size and Stability of Sputtered Metal Nanoparticles. *ACS Sustainable Chem. Eng.* 8, 18167–18176. doi:10.1021/acssuschemeng.0c06549

Orozco-Montes, V., Caillard, A., Brault, P., Chamorro-Coral, W., Bigarre, J., Sauldubois, A., et al. (2021). Synthesis of Platinum Nanoparticles by Plasma Sputtering onto Glycerol: Effect of Argon Pressure on Their Physicochemical Properties. *J. Phys. Chem. C* 125, 3169–3179. doi:10.1021/acs.jpcc.0c09746

Patel, V. R., Dumancas, G. G., Viswanath, L. C. K., Maples, R., and Subong, B. J. J. (2016). Castor Oil: Properties, Uses, and Optimization of Processing Parameters in Commercial Production. *Lipid Insights* 9, 1–12. doi:10.4137/LPI.S40233

Qadir, M. I., Kauling, A., Ebeling, G., Fartmann, M., Grehl, T., and Dupont, J. (2019). Functionalized Ionic Liquids Sputter Decorated With Pd Nanoparticles. *Aust. J. Chem.* 72, 49. doi:10.1071/CH18183

Sarakinos, K., Alami, J., and Konstantinidis, S. (2010). High Power Pulsed Magnetron Sputtering: A Review on Scientific and Engineering State of the Art. *Surf. Coat. Technol.* 204, 1661–1684. doi:10.1016/j.surfcoat.2009.11.013

Sebastian, V., Arruebo, M., and Santamaria, J. (2014). Reaction Engineering Strategies for the Production of Inorganic Nanomaterials. *Small* 10, 835–853. doi:10.1002/smll.201301641

Sergievskaya, A. P., Tatarchuk, V. V., Makotchenko, E. V., and Mironov, I. V. (2015). Formation of Gold Nanoparticles during the Reduction of HAuBr4 in Reverse Micelles of Oxyethylated Surfactant: Influence of Gold Precursor on the Growth Kinetics and Properties of the Particles. *J. Mater. Res.* 30, 1925–1933. doi:10.1557/jmr.2015.121

Sergievskaya, A., O'Reilly, A., Chauvin, A., Veselý, J., Panepinto, A., De Winter, J., et al. (2021). Magnetron Sputter Deposition of Silver onto castor Oil: The Effect of Plasma Parameters on Nanoparticle Properties. *Colloids Surf. A: Physicochem. Eng. Aspects* 615, 126286. doi:10.1016/j.colsurfa.2021.126286

Shishino, Y., Yonezawa, T., Kawai, K., and Nishihara, H. (2010). Molten Matrix Sputtering Synthesis of Water-Soluble Luminescent Au Nanoparticles with a Large Stokes Shift. *Chem. Commun.* 46, 7211. doi:10.1039/c0cc01702g

Shishino, Y., Yonezawa, T., Udagawa, S., Hase, K., and Nishihara, H. (2011). Preparation of Optical Resins Containing Dispersed Gold Nanoparticles by the Matrix Sputtering Method. *Angew. Chem.* 123, 729–731. doi:10.1002/ange.201005723

Slepička, P., Elashnikov, R., Ulbrich, P., Staszek, M., Kolská, Z., and Švorčík, V. (2015). Stabilization of Sputtered Gold and Silver Nanoparticles in PEG Colloid Solutions. *J. Nanopart. Res.* 17. doi:10.1007/s11051-014-2850-z

Sugioka, D., Kameyama, T., Kuwabata, S., and Torimoto, T. (2015). Single-step Preparation of Two-Dimensionally Organized Gold Particles via Ionic Liquid/Metal Sputter Deposition. *Phys. Chem. Chem. Phys.* 17, 13150–13159. doi:10.1039/c5cp01602a

Sumi, T., Motono, S., Ishida, Y., Shirahata, N., and Yonezawa, T. (2015). Formation and Optical Properties of Fluorescent Gold Nanoparticles Obtained by Matrix Sputtering Method with Volatile Mercaptan Molecules in the Vacuum Chamber and Consideration of Their Structures. *Langmuir* 31, 4323–4329. doi:10.1021/acs.langmuir.5b00294

Suzuki, T., Okazaki, K.-i., Kiyama, T., Kuwabata, S., and Torimoto, T. (2009). A Facile Synthesis of AuAg Alloy Nanoparticles Using a Chemical Reaction Induced by Sputter Deposition of Metal onto Ionic Liquids. *Electrochemistry* 77, 636–638. doi:10.5796/electrochemistry.77.636

Talapin, D. V., Lee, J.-S., Kovalenko, M. V., and Shevchenko, E. V. (2010). Prospects of Colloidal Nanocrystals for Electronic and Optoelectronic Applications. *Chem. Rev.* 110, 389–458. doi:10.1021/cr900137k

Thanh, N. T. K., Maclean, N., and Mahiddine, S. (2014). Mechanisms of Nucleation and Growth of Nanoparticles in Solution. *Chem. Rev.* 114, 7610–7630. doi:10.1021/cr400544s

Torimoto, T., Okazaki, K.-i., Kiyama, T., Hirahara, K., Tanaka, N., and Kuwabata, S. (2006). Sputter Deposition onto Ionic Liquids: Simple and Clean Synthesis of Highly Dispersed Ultrafine Metal Nanoparticles. *Appl. Phys. Lett.* 89, 243117. doi:10.1063/1.2404975

Torimoto, T., Kameyama, T., and Kuwabata, S. (2016). "Top-Down Synthesis Methods for Nanoscale Catalysts," in *Nanocatalysis In Ionic Liquids*. Weinheim, Germany: Wiley-VCH Verlag GmbH & Co. KGaA, 171–205. doi:10.1002/9783527693283.ch9

Tsuda, T., Yoshii, K., Torimoto, T., and Kuwabata, S. (2010). Oxygen Reduction Catalytic Ability of Platinum Nanoparticles Prepared by Room-Temperature Ionic Liquid-Sputtering Method. *J. Power Sourc.* 195, 5980–5985. doi:10.1016/j.jpowsour.2009.11.027

Van Aeken, K., Mahieu, S., and Depla, D. (2008). The Metal Flux from a Rotating Cylindrical Magnetron: A Monte Carlo Simulation. *J. Phys. D: Appl. Phys.* 41, 205307. doi:10.1088/0022-3727/41/20/205307

Vanecht, E., Binnemans, K., Seo, J. W., Stappers, L., and Fransaer, J. (2011). Growth of Sputter-Deposited Gold Nanoparticles in Ionic Liquids. *Phys. Chem. Chem. Phys.* 13, 13565–13571. doi:10.1039/c1cp20552h

Vanecht, E., Binnemans, K., Patskovsky, S., Meunier, M., Seo, J. W., Stappers, L., et al. (2012). Stability of Sputter-Deposited Gold Nanoparticles in Imidazolium Ionic Liquids. *Phys. Chem. Chem. Phys.* 14, 5662. doi:10.1039/c2cp23677j

Wagener, M., Murty, B. S., and Günther, B. (1996). Preparation of Metal Nanosuspensions by High-Pressure DC-Sputtering on Running Liquids. *MRS Proc.* 457, 149. doi:10.1557/PROC-457-149

Wang, F., Richards, V. N., Shields, S. P., and Buhro, W. E. (2014). Kinetics and Mechanisms of Aggregative Nanocrystal Growth. *Chem. Mater.* 26, 5–21. doi:10.1021/cm402139r

Watzky, M. A., and Finke, R. G. (1997). Transition Metal Nanocluster Formation Kinetic and Mechanistic Studies. A New Mechanism When Hydrogen is the Reductant: Slow, Continuous Nucleation and Fast Autocatalytic

Surface Growth. *J. Am. Chem. Soc.* 119, 10382–10400. doi:10.1021/ja9705102

Watzky, M. A., and Finke, R. G. (2018). Gold Nanoparticle Formation Kinetics and Mechanism: A Critical Analysis of the "Redox Crystallization" Mechanism. *ACS Omega* 3, 1555–1563. doi:10.1021/acsomega.7b01772

Wender, H., De Oliveira, L. F., Feil, A. F., Lissner, E., Migowski, P., Meneghetti, M. R., et al. (2010). Synthesis of Gold Nanoparticles in a Biocompatible Fluid from Sputtering Deposition Onto Castor Oil. *Chem. Commun.* 46, 7019–7021. doi:10.1039/c0cc01353f

Wender, H., Gonçalves, R. V., Feil, A. F., Migowski, P., Poletto, F. S., Pohlmann, A. R., et al. (2011). Sputtering onto Liquids: From Thin Films to Nanoparticles. *J. Phys. Chem. C* 115, 16362–16367. doi:10.1021/jp205390d

Wender, H., Migowski, P., Feil, A. F., Teixeira, S. R., and Dupont, J. (2013). Sputtering Deposition of Nanoparticles onto Liquid Substrates: Recent Advances and Future Trends. *Coord. Chem. Rev.* 257, 2468–2483. doi:10.1016/j.ccr.2013.01.013

Conflict of Interest: The authors declare that the research was conducted in the absence of any commercial or financial relationships that could be construed as a potential conflict of interest.

Publisher's Note: All claims expressed in this article are solely those of the authors and do not necessarily represent those of their affiliated organizations, or those of the publisher, the editors and the reviewers. Any product that may be evaluated in this article, or claim that may be made by its manufacturer, is not guaranteed or endorsed by the publisher.